Colloidal Quantum Dot Photovoltaics: A Path Forward

Illan J. Kramer and Edward H. Sargent*

Department of Electrical and Computer Engineering, University of Toronto, 10 King's College Road, Toronto, Ontario M5S 3G4, Canada

ABSTRACT Colloidal quantum dots (CQDs) offer a path toward high-efficiency photovoltaics based on low-cost materials and processes. Spectral tunability *via* the quantum size effect facilitates absorption of specific wavelengths from across the sun's broad spectrum. CQD materials' ease of processing derives from their synthesis, storage, and processing in solution. Rapid advances have brought colloidal quantum dot photovoltaic solar power conversion efficiencies of 6% in the latest reports. These achievements represent important first steps toward commercially compelling performance. Here we review advances in device architecture and materials science. We diagnose the principal phenomenon—electronic states within the CQD film band gap that limit both current and voltage in devices—that must be cured for CQD PV devices to fulfill their promise. We close with a prescription, expressed as bounds on the density and energy of electronic states within the CQD film band gap, that should allow device efficiencies to rise to those required for the future of the solar energy field.

KEYWORDS: quantum dot · nanocrystal · mobility · defect density · monodispersity · architecture · diffusion · solar cell · photovoltaic

First- and second-generation photovoltaics (PV)[1] are composed of well-understood materials such as crystalline silicon (c-Si) and cadmium telluride (CdTe), respectively. Despite great progress on performance and cost in these technologies, there remains a keen interest in defining pathways to technologies that offer cost per watt-peak ($/$W_P$) of electrical power generated that will compete, unsubsidized, with legacy electricity generation technologies.

Organic and other low-temperature solution-processed solar technologies have also seen great strides. Present-day power conversion efficiencies (η) of the best organic and polymer solar cells, combined with low materials and manufacturing costs, enable remarkably low costs per watt-peak at the module level. However, in all solar technologies, it is imperative to account also for balance of systems (BoS) costs associated with complete installations. BoS costs include factors such as the mechanical racking, installation labor, inverters, and other mechanical and electrical components. The installed cost in ($/$W_P$) is given by eq 1:

$$\text{cost}_{\text{installed}} = \frac{\text{cost}_{\text{module}}/\text{m}^2 + \text{BoS}/\text{m}^2}{\eta \cdot \text{Incident Light Intensity}} \quad (1)$$

An extreme example illustrates the need for solar cells to exceed a certain threshold efficiency in order to be economically compelling. Aggressive forecasts for BoS reduction foresee $100/m^2 costs within a coming decade.[2] A low-cost solar module technology offering 10% power conversion efficiency can, in view of the sun's 1000 W/m^2 peak insolation, offer in the best case $1/$W_P$, *in the limit of zero module cost.*

This extreme illustration, one in which the module maker earns zero revenue, leads to a compelling installed cost. Using more feasible numbers from the module producer's perspective, such as a still-aggressive target module cost of $0.5/$W_P$, and the same aggressive BoS cost of $0.5/$W_P$, leads to the same compelling installed cost of $1/$W_P$. This more feasible illustration demands a 20% solar power conversion efficiency at a module level.

In sum, finite BoS cost has one unavoidable implication: if cost and efficiency can to some degree be traded off, they can only be exchanged down to some minimum acceptable threshold efficiency. While experts differ on the precise figures, it is easy to see that any solar technology that is in its development stages today must offer a clear path to 15% or greater solar power conversion efficiency, no matter how low its module cost.

Colloidal Quantum Dot Photovoltaics. CQDs are semiconductor nanoparticles synthesized in, and processed from, the solution phase. Their processing into thin films is most often carried out at or near room temperature. These materials offer strong optical absorption due to the direct band-gap as well as the light weight and low materials and fabrication costs featured in third-generation photovoltaic technologies.

* Address correspondence to ted.sargent@utoronto.ca.

Received for review September 6, 2011 and accepted October 3, 2011.

Published online October 03, 2011
10.1021/nn203438u

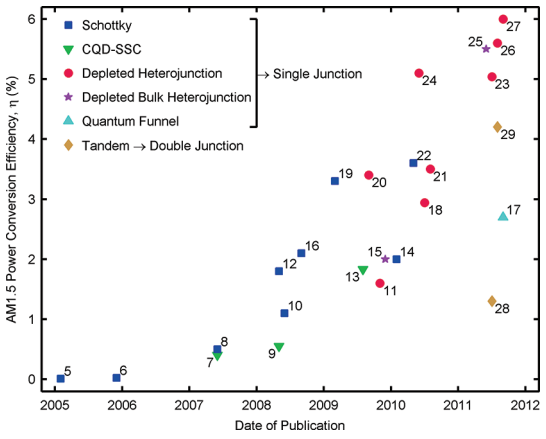

Figure 1. CQD PV performance progress since 2005. Blue squares = Schottky, green triangles = CQD-sensitized solar cells, red circles = depleted heterojunction, purple stars = depleted bulk heterojunction, and cyan upward triangle = quantum funnel. The best AM1.5 device efficiency achieved has been η = 6%. Gold diamonds represent tandem (double-junction) architectures with the efficiency of the best device achieving η = 4.2%. Each point is labeled with the corresponding reference number.

Importantly, CQDs also offer an avenue to high efficiency *via* optimal utilization of the sun's broad spectrum. While this article will later discuss significant materials engineering challenges that remain, CQDs' capacity to be band-gap-tuned to spectral positions optimal for efficient visible and infrared harvesting ensures that there exist no fundamental obstacles to achieving compelling high solar power conversion efficiencies.

Quantum dots' band gap is readily tuned, at the time of synthesis, simply by changing the nanoparticles' physical dimensions. This feature facilitates the use of a single materials system to fabricate multiple-junction solar cells—photovoltaic devices consisting of a number of different band gap materials, each optimized to the efficient conversion of energy within a limited spectral band. Whereas single-junction solar cells are fundamentally limited to 31% ultimate solar power conversion efficiency at 1 sun, optimal tandem cells offer an efficiency asymptote of 42% and triple-junction of 49%.[3,4] Thus, once successfully engineered to fulfill even a reasonable portion of its underlying potential, CQD solar technology offers a strategy to increasingly high efficiencies that overcome the inevitability of finite BoS costs.

Recent Progress in CQD PV. The ultimate performance figure of merit of a solar cell—its power conversion efficiency, η—can be deconstructed into three multiplicative components: short-circuit current density (J_{SC}), open-circuit voltage (V_{OC}) and fill factor (FF) as shown in eq 2

$$\eta_{AM1.5} = \frac{J_{SC} \times V_{OC} \times FF \times A}{P_{in}} \qquad (2)$$

VOCABULARY: CQD—colloidal quantum dot • **J_{SC}**—short-circuit current density • **V_{OC}**—open-circuit voltage • **FF**—fill factor • **R_S**—series resistance • **R_{SH}**—shunt resistance • **η**—power conversion efficiency • **AM1.5**—air mass 1.5 spectra • **P_{IN}**—incident optical power • **IQE**—internal quantum efficiency (aka absorbed photon conversion efficiency) • **SSC**—sensitized solar cell • **DH**—depleted heterojunction • **DBH**—depleted bulk heterojunction • **GRL**—graded recombination layer • **TCO**—transparent conductive oxide • **ITO**—indium tin oxide • **FTO**—fluorine-doped tin oxide • **MEG**—multiple exciton generation • **μ**—mobility • **N_t**—trap state density • **MCC**—metal chalcogenide complexes • **FET**—field effect transistor.

where P_{in} is the incident optical power, A is the device area, and the subscript AM1.5 is the solar insolation (both in intensity and spectrum) standard.

The η has progressed in the past six years from sub-1% in early reports[5−9] through the low single digits[10−22] to over 5%[23−26] and most recently a 6%[27] report. Within the last year, there has also been progress on multiple-junction CQD solar cells to over 4%.[28,29] Figure 1 illustrates this progress graphically.

These rapid advances have been achieved through two general categories of improvement. First, there has been an increased depth of knowledge in the materials science of CQD thin films. This includes the development of new types of CQD materials,[10,12,19,30,31] progress in understanding the electronic transport and recombination mechanisms at play in CQD films,[32−37] and innovations in materials processing that have led to correspondingly enhanced electronic materials properties (Figure 2).[27,38,39] In parallel, device architectures (Figures 2 and 3) have progressed in response to the potential and the present-day limitations of CQD films viewed as prospective photovoltaic materials (Table 1).

In this review, we first describe the innovative device designs that have been used to date and outline the most promising designs for moving the performance bar further forward. We will then describe the advances in materials chemistry and characterization that will support existing architectures and enable new and improved strategies.

Improving Performance through Device Architecture Innovations. Early progress in CQD PV device performance was achieved through engineering of the readily fabricated Schottky CQD solar cell.[10,12,14,16,22] A thin film of CQDs is contacted ohmically on one side *via* a transparent conductive oxide (TCO) and on the other side using a shallow work function metal at which a significant built-in potential is established relative to the (natively p-type) CQD film. Indium tin oxide (ITO) is typically used as the ohmic TCO, while aluminum and magnesium have been widely used as the shallow work function metal. Figure 2a shows the device architecture along with a corresponding spatial band diagram.

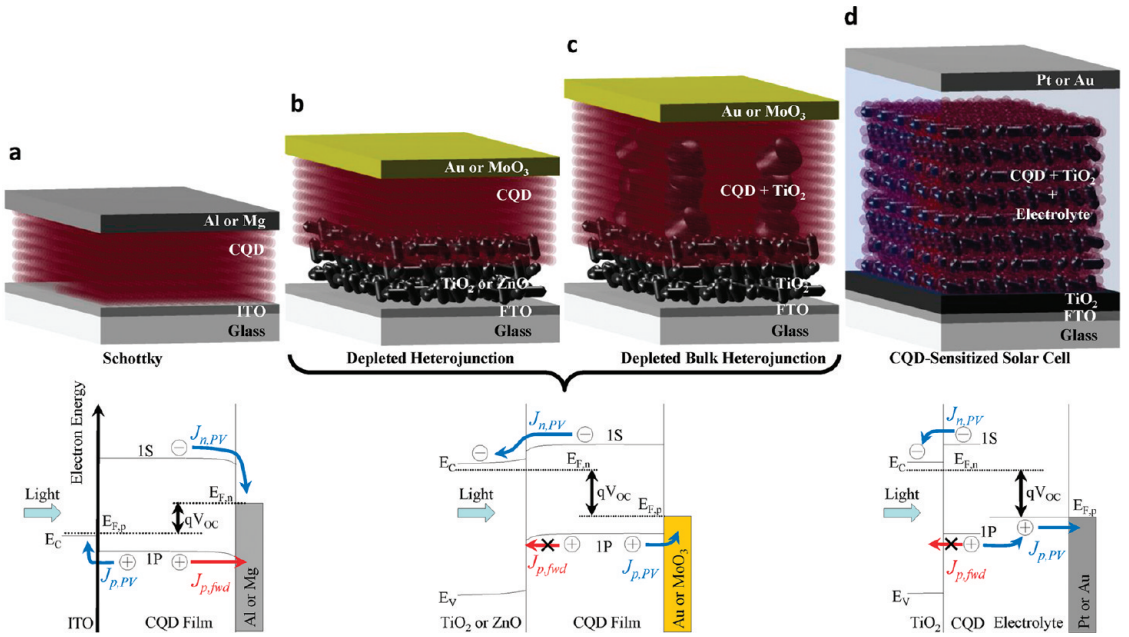

Figure 2. Single-junction CQD solar cell architectures. (a) Schottky CQD solar cell. (b) Depleted heterojunction CQD solar cell. (c) Depleted bulk heterojunction CQD solar cell. (d) CQD-sensitized solar cell. Also shown are the electron band diagrams of each architecture as indicated. Note that the depleted heterojunction and depleted bulk heterojunction solar cells share the same band diagram, with the only difference being the larger volume of CQDs within the depletion region due to the interfacial higher surface area between the TiO_2 and CQD film.

TABLE 1. Features and Challenges in CQD PV

feature	challenges
inexpensive to synthesize and process	difficult to dope controllably
light weight	low charge carrier mobility
processable from solution	high surface trap density
processable at low temperatures	incomplete mechanistic understanding of transport and recombination
strongly optically absorbing	synthesis dependence of materials behavior incompletely understood
band gap tunable *via* size-effect tuning	

In parallel, CQD-sensitized solar cells (CQD-SSCs)[7,13] emerged from the foundations of dye-sensitized solar cells (DSSCs)[40] and take similar advantage of the high interfacial areas between a nanoporous TCO, such as TiO_2 or ZnO, and the light absorbing material. By substituting CQDs for the molecular dye typically found in DSSCs, it is possible to extend the absorptive range beyond the cutoff wavelengths of ruthenium-based dyes. CQDs absorb light, whereupon excitons dissociate, with rapid electron injection into the TiO_2 and hole extraction to the platinum back contact through an electrolyte. Figure 2d shows the device architecture along with the corresponding electron band diagram.

CQD PV reached above 5% solar power conversion efficiency for the first time with the advent of the depleted heterojunction (DH)[11,18,20,21,23,24,26,27] architecture (Figure 2b). DH devices coat a wide-band-gap semiconductor such as TiO_2 or ZnO with CQDs. In contrast with CQD-SSCs, and in resemblance with Schottky CQD cells, DH devices exploit transport of electrons and holes through a many-layer CQD film.

Today, this ambipolar transport occurs successfully (*i.e.*, without undue recombination) over a distance equal to the sum of a depletion region and a minority carrier diffusion length—typically limiting the current-contributing CQD layer thickness to 100–300 nm. While CQD films can absorb nearly all visible wavelength light in a single pass through this thickness, near-infrared colors are only partially absorbed. This limitation may be termed an absorption *versus* extraction trade-off arising from electronic transport limits in CQD films further detailed below.

Depleted bulk heterojunctions (DBH)[15,25] (Figure 2c) provide an architecture solution to this present-day materials limitation: they employ an infiltrated nanoporous architecture to extend the photon interaction length while maintaining a short exit route for electrons. Electrons, the current-limiting carrier in most CQD solar cells, are collected laterally into the nearest vertical instance of the TiO_2 or ZnO matrix.

Tandem and multijunction solar cells exploit facile layering of size-effect-tuned quantum dot layers

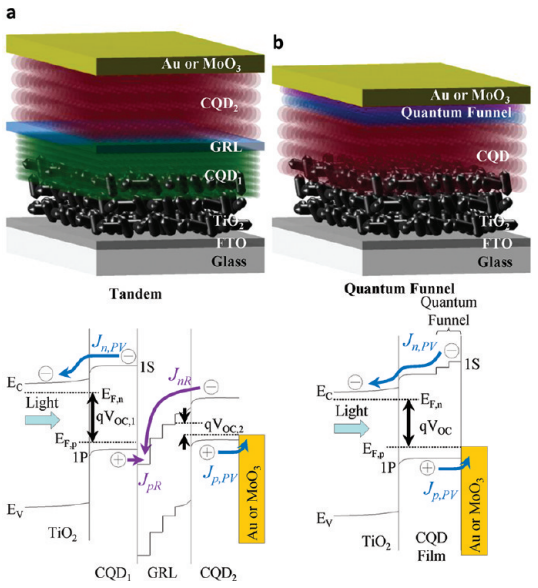

Figure 3. (a) Device architecture and band diagram for the tandem CQD cell using a graded recombination layer (GRL). The different sizes and colors of the representative CQD layers illustrate that different sizes of CQDs were used for junctions 1 and 2 within the tandem architecture. Purple arrows indicate the location of recombination of holes from the front cell and electrons from the back cell. J_{pR} and J_{nR} must be equal in order to satisfy the current matching condition and thus get voltage addition. (b) Device architecture and band diagram for the quantum funnel solar cell where different sizes and colors of the representative CQD layers illustrate that different sizes of CQDs were used to form the quantum funnel.

having multiple, different, optimally chosen band gaps.[28,29] The tandem cells reported employ two stacked DH cells, where the upper metal contact of the bottom cell and lower transparent contact of the top cell are replaced using a transparent, carefully engineered recombination layer. The recombination layer enables holes generated in the bottom cell to recombine with electrons generated in the top cell, maintaining charge neutrality in the overall device and facilitating current matching. These first reports utilize CQDs with band gaps close to the two ideal tandem band gaps.[3] Further progress will be achieved once the electron-accepting electrodes are optimized for the band structures of these quantum-tuned light absorbers.[26] Figure 3a shows the device architecture and corresponding electron band diagram with purple arrows indicating the location of recombination of holes from the front cell with electrons from the back cell.

Band gap engineering of colloidal quantum dots began with optical-domain studies of materials and films.[41] Building on these advances, early efforts at engineering optoelectronic devices based on multiple sizes of colloidal quantum dots were postulated and initiated.[42−46] A new band-gap-engineered device architecture known as the quantum funnel solar cell has recently showcased the advantages of multi-band-gap

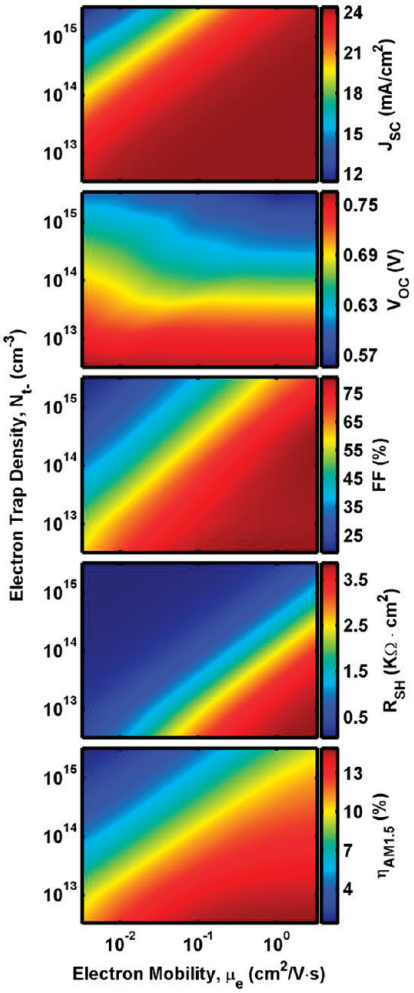

Figure 4. Modeled performance of the depleted heterojunction device as a function of electron trap density and carrier mobility.

CQD structures in enabling enhanced device performance.[17] This report—the first to utilize tunability *within* a given active layer—describes how a cascaded energy profile in the conduction band of the CQD film selectively guides electrons to the electron-accepting contact. This enables more efficient extraction of charge carriers generated in the undepleted quasi-neutral region in which minority carrier diffusion is, at present, inefficient. Because size-effect tuning primarily influences the conduction band in PbS CQDs,[47,26] electron transport is enhanced without impeding hole flow. Enhanced quasi-neutral carrier collection is an essential ingredient in breaking the absorption *versus* extraction compromise inherent in the DH architecture. Figure 3b depicts the device architecture with different sizes of CQDs near the back contact depicting the quantum funnel. The accompanying band diagram shows the energy cascade in the conduction band provided by the quantum funnel.

While much progress has been made, much opportunity remains for further advances in CQD PV device architecture. One area of interest will be achievable once it is possible to dope CQD films controllably,

TABLE 2. Roadmap to Improved Single-Junction CQD PV Performance[a]

			experimental results		model prediction	
	parameter		6%[27*]	N/A[54**]	10%	15%
CQD film	band edge electron mobility ($cm^2/V \cdot s$)		0.03	16	0.1	0.4
	band edge hole mobility ($cm^2/V \cdot s$)		0.03		0.1	0.4
	majority free carrier density (cm^{-3})		4×10^{15}	1×10^{16}	1×10^{16}	1×10^{16}
	conduction band	trap energy below CB (eV)	0.25[‡]		0.22	0.15
		trap density (cm^{-3})	5×10^{14}[‡]		9×10^{13}	8×10^{12}
	valence band	trap energy above VB (eV)	0.25[‡]		0.22	0.15
		trap density (cm^{-3})	5×10^{14}[‡]		9×10^{13}	8×10^{12}
electrode	mobility ($cm^2/V \cdot s$)		2.4		2.4	2.4
	free carrier density (cm^{-3})		1×10^{16}		1×10^{16}	1×10^{16}

[a] * = atomic ligands; ** = MCC ligands; ‡ = Trap energies based on spectroscopic measurements[27]; trap densities estimated to match performance in model.

either n-type or p-type. A p−n homojunction could offer to expand the dimensions of the depletion region, making it double-sided, thus further enhancing efficient carrier collection. A recent p−n nanoparticle-based solar cell offers a taste of this possibility:[48] Bi_2S_3 bulk nanoparticles serve as an n-type layer and PbS CQDs as a p-type layer. The field awaits the improvements in J_{SC}, FF, and particularly V_{OC} that may be achieved once this architecture and its constituent materials are fully engineered.

Two physical mechanisms have attracted great interest in the CQD community: hot carrier collection and multiple exciton generation (MEG). Hot carriers include photogenerated electrons that have yet to relax to the band edge. If these carriers can be extracted from the CQD material, then an enhancement in open-circuit voltage can be expected since the energy of thermalization need no longer be sacrificed. Hot electrons have recently been shown to inject from PbSe CQDs into TiO_2.[37] The field awaits with considerable interest the realization of solar cells that take advantage of this phenomenon.

In MEG, a single high-energy photon generates multiple lower-energy excitons, the latter possessing the band gap energy. Here the challenge is to harvest these multiple excitons before they recombine *via* rapid processes such as Auger recombination. If it can be successfully implemented in a CQD PV device, MEG offers the prospect of multijunction performance (*i.e.*, beyond the theoretical Schockley−Quiesser limits[49]) in a single-junction device. The internal quantum efficiency (IQE, also known as the absorbed photon conversion efficiency) provides a metric to quantify the current output for each absorbed photon as defined by eq 3.

$$\mathrm{IQE}(\lambda) = \frac{hc}{\lambda} \times \frac{I_{OUT}}{P_{IN} \times \%\mathrm{Abs}(\lambda)} \times 100\% \qquad (3)$$

where h is Planck's constant, c is the speed of light, I_{OUT} is the output current, P_{IN} is the input optical power, and $\%\mathrm{Abs}(\lambda)$ is the percentage of power absorbed at the wavelength, λ. Recent claims of greater-than-unity IQE in a CQD device have attracted interest in light of this prospect.[50] A topic of ongoing research is the question of whether CQD films provide enhanced multiple exciton generation relative to their bulk counterparts.[51]

Improving CQD PV Performance through Materials Science. We now turn to the engineering of CQD materials that meet the demanding requirements of photovoltaic device engineering.

The transport and recombination parameters of a CQD film must be enhanced to allow for efficient extraction of the carriers generated by every absorbed photon. The key optical property of a CQD film is its absorption per unit length, which one desires to maximize above the semiconductor film's cutoff, or band gap.

CQD films have large absorption coefficients that enable close to complete above band gap absorption in a material having $\sim 1\ \mu$m thickness. Unfortunately, with minority carrier diffusion lengths reported to date residing more on the order of tens of nanometers,[32] extraction is efficient only in the presence of a significant built-in electric field. The majority of current in CQD today is thus dominated by drift instead of diffusion.

While these have yet to be comprehensively characterized and catalogued, it is expected that CQD films will, largely because of their abundant surface area, present many opportunities for the formation of electronic traps.[52] Midgap states can capture both electrons and holes, accelerating recombination. Shallow traps, while less fatal, do impede transport, leading to activated hopping, and may also limit quasi-Fermi level separation necessary to the establishment of a large V_{OC}.

In Table 2, we propose an illustrative roadmap, tracing the path from present-day PV materials properties and efficiencies toward high single-junction device performance. PV efficiency steadily increases as minority carrier trap energy depth and density are decreased. Included also are state-of-art materials properties of CQD films that account for the present-day

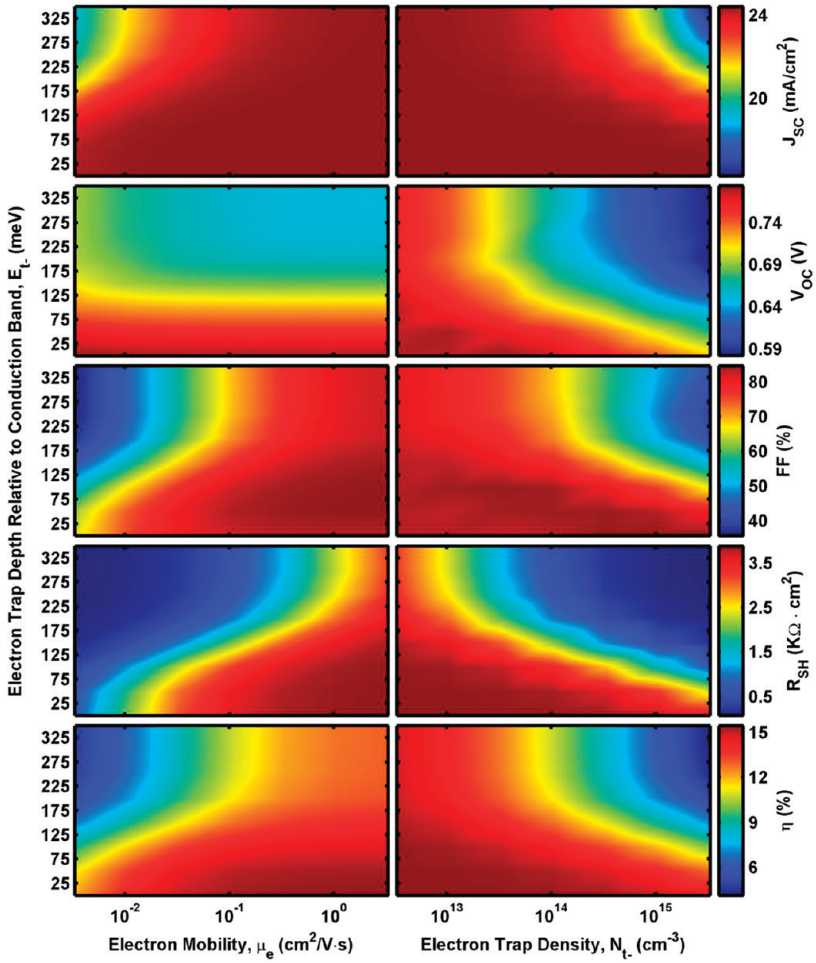

Figure 5. Modeled performance of the depleted heterojunction device as a function of trap depth and either minority carrier mobility (left column) or trap density (right column).

record of 6% efficiency. In all modeling results, traps are represented by the single specified trap energy level and density shown in the table. In the table and the figures that follow, mobilities are represented as band edge mobility values such as are typically extracted from FET characteristics: the effect of shallow traps is to produce an effective mobility smaller than this band edge mobility *via* repeated trapping and delayed emission.

This same optoelectronic model was employed to generate the results of Figures 4, 5, and 6. The performance metrics are considered within four main categories: J_{SC}, V_{OC}, FF, and $\eta_{AM1.5}$. The contributors to FF are further in the form of the shunt resistance (R_{SH}) and series resistance (R_S).

As seen in Figure 4, decreasing trap state energy and increasing the band edge mobility have similarly beneficial effects on most parameters—hence the diagonal equi-efficiency lines as a function of these two orthogonally represented parameters. The exception is open-circuit voltage, which is limited by trap state densities instead of by band edge mobilities. Photogenerated carriers that are consumed filling trap states diminish quasi-Fermi splitting, hence *V*oc.

Figure 5 introduces the additional crucial parameter of trap state energy depth. Once again, band edge mobility and trap state depth can be traded off against one another from the point of view of current but not in the achievement of the open-circuit voltage needed for high efficiency. Fortunately, once a sufficiently low trap state density ($<10^{13}$ cm^{-3}) is reached, these few remaining traps can be deep (0.3 eV) without impeding the achievement of >14% single-junction power conversion efficiency.

Figure 6 investigates the role of device thickness. As expected, increasing the thickness of planar devices will provide compelling performance advantages once mobilities, trap state densities, and trap state depths are all brought suitably under control.

CQD Materials Characterization For PV Performance. We now discuss materials characterization techniques to identify the presence of these deep traps and quantify critical parameters such as free carrier mobility. There are many techniques used today to determine these characteristic values. They include time-of-flight

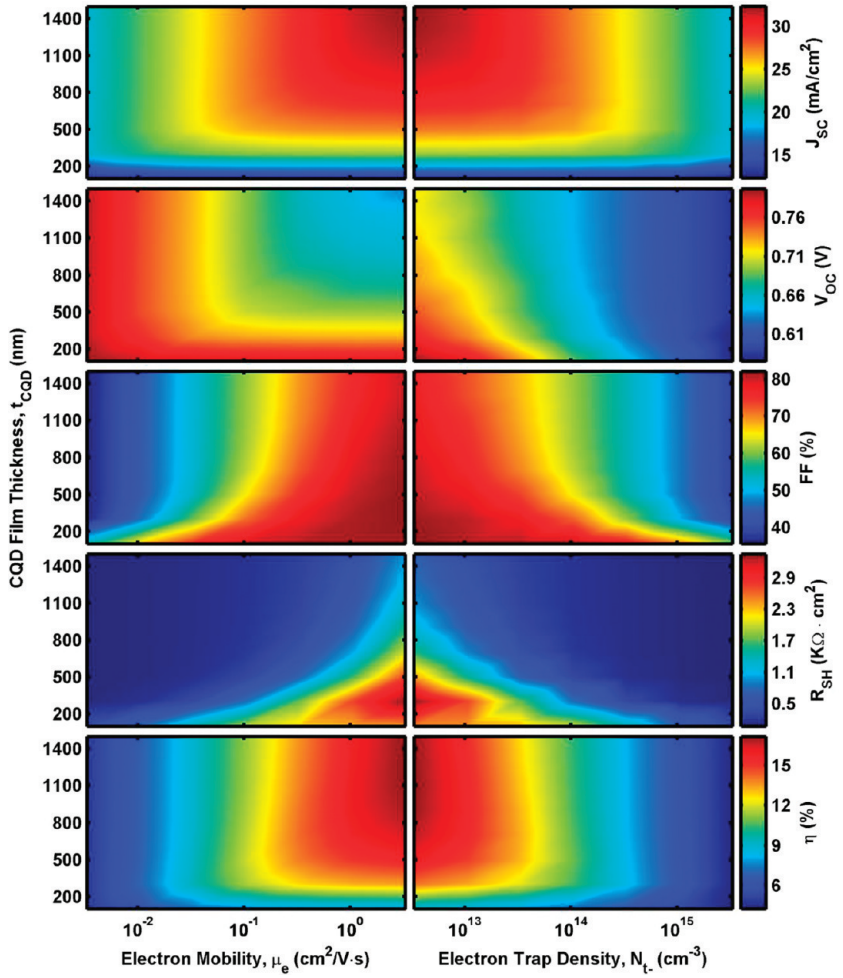

Figure 6. Modeled performance of the depleted heterojunction device as a function of device thickness and minority carrier mobility (left column) and trap density (right column).

(TOF),[32] carrier extraction through linearly increasing voltage (CELIV),[32] admittance spectroscopy,[53] and capacitance–voltage measurements.[24] All of these experiments involve the fabrication of rectifying junctions such as Schottky or DH devices, taking them beyond the realm of straightforward materials characterization. We instead put a focus herein on two characterization techniques that do not require the fabrication of solar cells.

The first simple tool is photoluminescence (PL). This technique only probes optically active states and therefore results in a very weak signal in materials having high densities of midgap states. In addition to highlighting, through its relative intensity, the presence or absence of recombination mechanisms that will lessen PV device efficiency, PL can, through the observation of (desirably) small Stokes shifts *versus* (undesirably) large ones, indicate whether a material is likely to provide a large V_{OC}.

Field effect transistor (FET)[54–56] measurements provide a ready means to evaluate transport properties in CQD films. Here we emphasize as well the caution that must be exercised in interpreting FET mobilities in the context of PV materials' promise. The transconductance slope allows the extraction of charge carrier mobility through the conduction or valence bands, while the subthreshold slope (S) offers a glimpse at the integrated density of trap states. S is defined[57] in eq 4 as

$$S = \frac{kT}{q\log(e)}\left[1 + \frac{qx_i}{\varepsilon_i}\left(\sqrt{\varepsilon_s N_{t-}} + qN_{\text{int}}\right)\right] \qquad (4)$$

where e is Euler's number, k is the Boltzmann constant, q is the elementary charge, T is the temperature, x_i is the gate dielectric thickness, ε_i and ε_s are the gate dielectric and CQD dielectric constants, respectively, and N_{t-} and N_{int} are the bulk and interface states of the CQD film and CQD/gate dielectric interface, respectively. Equation 4 does not allow for independent determination of bulk states and interface states but allows for an upper bound on both when the other is taken to be zero.

We note that both linear and saturated mobilities typically correspond to band edge values presented in the figures above, and thus even high values do not, on their own, confirm the sufficiency of a material in

photovoltaic applications. On the other hand, achieving high mobilities (>1 $cm^2/(V \cdot s)$) combined with low subthreshold slope (ideally as close to the theoretical value of 60 mV/decade, more realistically in the hundreds of mV/decade) will suggest great promise.

CONCLUSIONS AND PERSPECTIVES

The field of CQD photovoltaics has moved forward at a rapid pace in recent years. The credit for these advances goes to synthetic and materials chemists, materials processing groups, and innovators in device architecture. Much progress remains to be achieved for commercially compelling efficiencies to be reached. In device engineering, architectures that increase absorption, decrease the requirement from long-distance transport, and exploit CQDs' band gap tunability offer considerable remaining promise. We propose that the full potential of CQD device performance will only be realized with breakthroughs at the materials level as well—principally in the control over surface passivation in CQD films. Innovative strategies in materials chemistry that result in a reduction in the density, and the energetic depth, of trap states will impact the CQD field—and the solar energy community in general—tremendously.

Acknowledgment. This publication is based on work in part supported by Award No. KUS-11-009-21, made by King Abdullah University of Science and Technology (KAUST). I.J.K. acknowledges the financial support through the Queen Elizabeth II/Ricoh Canada Graduate Scholarship in Science and Technology.

REFERENCES AND NOTES

1. Green, M. A. *Third Generation Photovoltaics: Advanced Solar Energy Conversion*; Springer-Verlag: Berlin, 2006.
2. *$1/W Photovoltaic Systems*; Department of Energy: Washington, DC, 2010.
3. Henry, C. H. Limiting Efficiencies of Ideal Single and Multiple Energy Gap Terrestrial Solar Cells. *J. Appl. Phys.* **1980**, *51*, 4494.
4. Sargent, E. H. Infrared Photovoltaics Made by Solution Processing. *Nat. Photonics* **2009**, *3*, 325–331.
5. McDonald, S. A.; Konstantatos, G.; Zhang, S.; Cyr, P. W.; Klem, E. J. D.; Levina, L.; Sargent, E. H. Solution-Processed PbS Quantum Dot Infrared Photodetectors and Photovoltaics. *Nat. Mater.* **2005**, *4*, 138–142.
6. Maria, A.; Cyr, P. W.; Klem, E. J. D.; Levina, L.; Sargent, E. H. Solution-Processed Infrared Photovoltaic Devices with >10% Monochromatic Internal Quantum Efficiency. *Appl. Phys. Lett.* **2005**, *87*, 213112.
7. Leschkies, K. S.; Divakar, R.; Basu, J.; Enache-Pommer, E.; Boercker, J. E.; Carter, C. B.; Kortshagen, U. R.; Norris, D. J.; Aydil, E. S. Photosensitization of ZnO Nanowires with CdSe Quantum Dots for Photovoltaic Devices. *Nano Lett.* **2007**, *7*, 1793–1798.
8. Klem, E. J. D.; MacNeil, D. D.; Cyr, P. W.; Levina, L.; Sargent, E. H. Efficient Solution-Processed Infrared Photovoltaic Cells: Planarized All-Inorganic Bulk Heterojunction Devices *via* Inter-Quantum-Dot Bridging During Growth from Solution. *Appl. Phys. Lett.* **2007**, *90*, 183113-3.
9. Mora-Seró, I.; Giménez, S.; Moehl, T.; Fabregat-Santiago, F.; Lana-Villareal, T.; Gómez, R.; Bisquert, J. Factors Determining the Photovoltaic Performance of a CdSe Quantum Dot Sensitized Solar Cell: The Role of the Linker Molecule and of the Counter Electrode. *Nanotechnology* **2008**, *19*, 424007.
10. Koleilat, G. I.; Levina, L.; Shukla, H.; Myrskog, S. H.; Hinds, S.; Pattantyus-Abraham, A. G.; Sargent, E. H. Efficient, Stable Infrared Photovoltaics Based on Solution-Cast Colloidal Quantum Dots. *ACS Nano* **2008**, *2*, 833–840.
11. Leschkies, K. S.; Beatty, T. J.; Kang, M. S.; Norris, D. J.; Aydil, E. S. Solar Cells Based on Junctions between Colloidal PbSe Nanocrystals and Thin ZnO Films. *ACS Nano* **2009**, *3*, 3638–3648.
12. Johnston, K. W.; Pattantyus-Abraham, A. G.; Clifford, J. P.; Myrskog, S. H.; MacNeil, D. D.; Levina, L.; Sargent, E. H. Schottky-Quantum Dot Photovoltaics for Efficient Infrared Power Conversion. *Appl. Phys. Lett.* **2008**, *92*, 151115.
13. Giménez, S.; Mora-Seró, I.; Macor, L.; Guijarro, N.; Lana-Villarreal, T.; Gómez, R.; Diguna, L. J.; Shen, Q.; Toyoda, T.; Bisquert, J. Improving the Performance of Colloidal Quantum-Dot-Sensitized Solar Cells. *Nanotechnology* **2009**, *20*, 295204.
14. Tang, J.; Wang, X.; Brzozowski, L.; Barkhouse, D. A. R.; Debnath, R.; Levina, L.; Sargent, E. H. Schottky Quantum Dot Solar Cells Stable in Air under Solar Illumination. *Adv. Mater.* **2010**, *22*, 1398–1402.
15. Leschkies, K. S.; Jacobs, A. G.; Norris, D. J.; Aydil, E. S. Nanowire-Quantum-Dot Solar Cells and the Influence of Nanowire Length on the Charge Collection Efficiency. *Appl. Phys. Lett.* **2009**, *95*, 193103.
16. Luther, J. M.; Law, M.; Beard, M. C.; Song, Q.; Reese, M. O.; Ellingson, R. J.; Nozik, A. J. Schottky Solar Cells Based on Colloidal Nanocrystal Films. *Nano Lett.* **2008**, *8*, 3488–3492.
17. Kramer, I. J.; Levina, L.; Debnath, R.; Zhitomirsky, D.; Sargent, E. H. Solar Cells Using Quantum Funnels. *Nano Lett.* **2011**, *11*, 3701–3706.
18. Luther, J. M.; Gao, J.; Lloyd, M. T.; Semonin, O. E.; Beard, M. C.; Nozik, A. J. Stability Assessment on a 3% Bilayer PbS/ZnO Quantum Dot Heterojunction Solar Cell. *Adv. Mater.* **2010**, *22*, 3704–3707.
19. Ma, W.; Luther, J. M.; Zheng, H.; Wu, Y.; Alivisatos, A. P. Photovoltaic Devices Employing Ternary PbS_xSe_{1-x} Nanocrystals. *Nano Lett.* **2009**, *9*, 1699–1703.
20. Choi, J. J.; Lim, Y.-F.; Santiago-Berrios, M. B.; Oh, M.; Hyun, B.-R.; Sun, L.; Bartnik, A. C.; Goedhart, A.; Malliaras, G. G.; Abruña, H. D.; *et al.* PbSe Nanocrystal Excitonic Solar Cells. *Nano Lett.* **2009**, *9*, 3749–3755.
21. Debnath, R.; Greiner, M. T.; Kramer, I. J.; Fischer, A.; Tang, J.; Barkhouse, D. A. R.; Wang, X.; Levina, L.; Lu, Z.-H.; Sargent, E. H. Depleted-Heterojunction Colloidal Quantum Dot Photovoltaics Employing Low-Cost Electrical Contacts. *Appl. Phys. Lett.* **2010**, *97*, 023109.
22. Debnath, R.; Tang, J.; Barkhouse, D. A.; Wang, X.; Pattantyus-Abraham, A. G.; Brzozowski, L.; Levina, L.; Sargent, E. H. Ambient-Processed Colloidal Quantum Dot Solar Cells *via* Individual Pre-encapsulation of Nanoparticles. *J. Am. Chem. Soc.* **2010**, *132*, 5952–5953.
23. Gao, J.; Perkins, C. L.; Luther, J. M.; Hanna, M. C.; Chen, H.-Y.; Semonin, O. E.; Nozik, A. J.; Ellingson, R. J.; Beard, M. C. n-Type Transition Metal Oxide as a Hole Extraction Layer in PbS Quantum Dot Solar Cells. *Nano Lett.* **2011**, *11*, 3263–3266.
24. Pattantyus-Abraham, A. G.; Kramer, I. J.; Barkhouse, A. R.; Wang, X.; Konstantatos, G.; Debnath, R.; Levina, L.; Raabe, I.; Nazeeruddin, M. K.; Grätzel, M.; *et al.* Depleted-Heterojunction Colloidal Quantum Dot Solar Cells. *ACS Nano* **2010**, *4*, 3374–3380.
25. Barkhouse, D. A. R.; Debnath, R.; Kramer, I. J.; Zhitomirsky, D.; Pattantyus-Abraham, A. G.; Levina, L.; Etgar, L.; Grätzel, M.; Sargent, E. H. Depleted Bulk Heterojunction Colloidal Quantum Dot Photovoltaics. *Adv. Mater.* **2011**, *23*, 3134–3138.
26. Liu, H.; Tang, J.; Kramer, I. J.; Debnath, R.; Koleilat, G. I.; Wang, X.; Fisher, A.; Li, R.; Brzozowski, L.; Levina, L.; *et al.* Electron Acceptor Materials Engineering in Colloidal Quantum Dot Solar Cells. *Adv. Mater.* **2011**, *23*, 3832–3837.
27. Tang, J.; Kemp, K. W.; Hoogland, S.; Jeong, K. S.; Liu, H.; Levina, L.; Furukawa, M.; Wang, X.; Debnath, R.; Cha, D.; *et al.* Colloidal-Quantum-Dot Photovoltaics Using Atomic-Ligand Passivation. *Nat. Mater.* **2011**, *10*, 765–771.

28. Choi, J. J.; Wenger, W. N.; Hoffman, R. S.; Lim, Y.; Luria, J.; Jasieniak, J.; Marohn, J. A.; Hanrath, T. Solution-Processed Nanocrystal Quantum Dot Tandem Solar Cells. *Adv. Mater.* **2011**, *23*, 3144–3148.
29. Wang, X.; Koleilat, G. I.; Tang, J.; Liu, H.; Kramer, I. J.; Debnath, R.; Brzozowski, L.; Barkhouse, D. A. R.; Levina, L.; Hoogland, S.; *et al.* Tandem Colloidal Quantum Dot Solar Cells Employing a Graded Recombination Layer. *Nat. Photonics* **2011**, *5*, 480–484.
30. Konstantatos, G.; Levina, L.; Tang, J.; Sargent, E. H. Sensitive Solution-Processed Bi_2S_3 Nanocrystalline Photodetectors. *Nano Lett.* **2008**, *8*, 4002–4006.
31. Puthussery, J.; Seefeld, S.; Berry, N.; Gibbs, M.; Law, M. Colloidal Iron Pyrite (FeS_2) Nanocrystal Inks for Thin-Film Photovoltaics. *J. Am. Chem. Soc.* **2011**, *133*, 716–719.
32. Johnston, K. W.; Pattantyus-Abraham, A. G.; Clifford, J. P.; Myrskog, S. H.; Hoogland, S.; Shukla, H.; Klem, E. J. D.; Levina, L.; Sargent, E. H. Efficient Schottky-Quantum-Dot Photovoltaics: The Roles of Depletion, Drift, and Diffusion. *Appl. Phys. Lett.* **2008**, *92*, 122111.
33. Tang, J.; Brzozowski, L.; Barkhouse, D. A. R.; Wang, X.; Debnath, R.; Wolowiec, R.; Palmiano, E.; Levina, L.; Pattantyus-Abraham, A. G.; Jamakosmanovic, D.; *et al.* Quantum Dot Photovoltaics in the Extreme Quantum Confinement Regime: The Surface-Chemical Origins of Exceptional Air- and Light-Stability. *ACS Nano* **2010**, *4*, 869–878.
34. Kang, M. S.; Sahu, A.; Norris, D. J.; Frisbie, C. D. Size-Dependent Electrical Transport in CdSe Nanocrystal Thin Films. *Nano Lett.* **2010**, *10*, 3727–3732.
35. Sukhovatkin, V.; Hinds, S.; Brzozowski, L.; Sargent, E. H. Colloidal Quantum-Dot Photodetectors Exploiting Multiexciton Generation. *Science* **2009**, *324*, 1542–1544.
36. Klar, T. A.; Franzl, T.; Rogach, A. L.; Feldmann, J. Super-Efficient Exciton Funneling in Layer-by-Layer Semiconductor Nanocrystal Structures. *Adv. Mater.* **2005**, *17*, 769–773.
37. Tisdale, W. A.; Williams, K. J.; Timp, B. A.; Norris, D. J.; Aydil, E. S.; Zhu, X.-Y. Hot-Electron Transfer from Semiconductor Nanocrystals. *Science* **2010**, *328*, 1543–1547.
38. Barkhouse, D. A. R.; Pattantyus-Abraham, A. G.; Levina, L.; Sargent, E. H. Thiols Passivate Recombination Centers in Colloidal Quantum Dots Leading to Enhanced Photovoltaic Device Efficiency. *ACS Nano* **2008**, *2*, 2356–2362.
39. Liu, Y.; Gibbs, M.; Puthussery, J.; Gaik, S.; Ihly, R.; Hillhouse, H. W.; Law, M. Dependence of Carrier Mobility on Nanocrystal Size and Ligand Length in PbSe Nanocrystal Solids. *Nano Lett.* **2010**, *10*, 1960–1969.
40. O'Regan, B.; Gratzel, M. A Low-Cost, High-Efficiency Solar Cell Based on Dye-Sensitized Colloidal TiO_2 Films. *Nature* **1991**, *353*, 737–740.
41. Franzl, T.; Klar, T. A.; Schietinger, S.; Rogach, A. L.; Feldmann, J. Exciton Recycling in Graded Gap Nanocrystal Structures. *Nano Lett.* **2004**, *4*, 1599–1603.
42. Morales-Acevedo, A. Variable Band-Gap Semiconductors as the Basis of New Solar Cells. *Sol. Energy* **2009**, *83*, 1466–1471.
43. Tsakalakos, L. Nanostructures for Photovoltaics. *Mater. Sci. Eng., R* **2008**, *62*, 175–189.
44. Weiss, E. A.; Chiechi, R. C.; Geyer, S. M.; Porter, V. J.; Bell, D. C.; Bawendi, M. G.; Whitesides, G. M. Size-Dependent Charge Collection in Junctions Containing Single-Size and Multi-Size Arrays of Colloidal CdSe Quantum Dots. *J. Am. Chem. Soc.* **2008**, *130*, 74–82.
45. Koeppe, R.; Bossart, O.; Calzaferri, G.; Sariciftci, N. S. Advanced Photon-Harvesting Concepts for Low-Energy Gap Organic Solar Cells. *Sol. Energy Mater. Sol. Cells* **2007**, *91*, 986–995.
46. Kamat, P. V. Quantum Dot Solar Cells. Semiconductor Nanocrystals as Light Harvesters. *J. Phys. Chem. C* **2008**, *112*, 18737–18753.
47. Hyun, B.-R.; Zhong, Y.-W.; Bartnik, A. C.; Sun, L.; Abruña, H. D.; Wise, F. W.; Goodreau, J. D.; Matthews, J. R.; Leslie, T. M.; Borrelli, N. F. Electron Injection from Colloidal PbS Quantum Dots into Titanium Dioxide Nanoparticles. *ACS Nano* **2008**, *2*, 2206–2212.
48. Rath, A. K.; Bernechea, M.; Martinez, L.; Konstantatos, G. Solution-Processed Heterojunction Solar Cells Based on p-Type PbS Quantum Dots and n-Type Bi_2S_3 Nanocrystals. *Adv. Mater.* **2011**, *23*, 3712–3717.
49. Shockley, W.; Queisser, H. J. Detailed Balance Limit of Efficiency of p–n Junction Solar Cells. *J. Appl. Phys.* **1961**, *32*, 510.
50. Sambur, J. B.; Novet, T.; Parkinson, B. A. Multiple Exciton Collection in a Sensitized Photovoltaic System. *Science* **2010**, *330*, 63–66.
51. Nair, G.; Chang, L.-Y.; Geyer, S. M.; Bawendi, M. G. Perspective on the Prospects of a Carrier Multiplication Nanocrystal Solar Cell. *Nano Lett.* **2011**, *11*, 2145–2151.
52. Voznyy, O. Mobile Surface Traps in CdSe Nanocrystals with Carboxylic Acid Ligands. *J. Phys. Chem. C* **2011**, *115*, 15927–15932.
53. Heath, J. T.; Cohen, J. D.; Shafarman, W. N. Distinguishing Metastable Changes in Bulk CIGS Defect Densities from Interface Effects. *Thin Solid Films* **2003**, *431–432*, 426–430.
54. Lee, J.-S.; Kovalenko, M. V.; Huang, J.; Chung, D. S.; Talapin, D. V. Band-like Transport, High Electron Mobility and High Photoconductivity in All-Inorganic Nanocrystal Arrays. *Nat. Nanotechnol.* **2011**, *6*, 348–352.
55. Talapin, D. V.; Murray, C. B. PbSe Nanocrystal Solids for n- and p-Channel Thin Film Field-Effect Transistors. *Science* **2005**, *310*, 86–89.
56. Dhar, B. M.; Özgün, R.; Dawidczyk, T.; Andreou, A.; Katz, H. E. Threshold Voltage Shifting for Memory and Tuning in Printed Transistor Circuits. *Mater. Sci. Eng., R* **2011**, *72*, 49–80.
57. Rolland, A.; Richard, J.; Kleider, J. P.; Mencaraglia, D. Electrical Properties of Amorphous Silicon Transistors and MIS-Devices: Comparative Study of Top Nitride and Bottom Nitride Configurations. *J. Electrochem. Soc.* **1993**, *140*, 3679–3683.